

## Article

# Effect of Stratification of Cathode Catalyst Layers on Durability of Proton Exchange Membrane Fuel Cells

Zikhona Nondudule <sup>1</sup>, Jessica Chamier <sup>2,\*</sup> and Mahabubur Chowdhury <sup>1</sup>

<sup>1</sup> Department of Chemical Engineering, Faculty of Engineering, Cape Peninsula University of Technology, Cape Town 7530, South Africa; 210237058@mycput.ac.za (Z.N.); chowdhurym@cput.ac.za (M.C.)

<sup>2</sup> Department of Chemical Engineering, Centre for Catalysis Research, HySA Catalysis, University of Cape Town, Cape Town 7700, South Africa

\* Correspondence: jessica.chamier@uct.ac.za; Tel.: +27-(0)-21-650-2515

**Abstract:** To decrease the cost of fuel cell manufacturing, the amount of platinum (Pt) in the catalyst layer needs to be reduced. In this study, ionomer gradient membrane electrode assemblies (MEAs) were designed to reduce Pt loading without sacrificing performance and lifetime. A two-layer stratification of the cathode was achieved with varying ratios of 28 wt. % ionomer in the inner layer, on the membrane, and 24 wt. % on the outer layer, coated onto the inner layer. To study the MEA performance, the electrochemical surface area (ECSA), polarization curves, and electrochemical impedance spectroscopy (EIS) responses were evaluated under 20, 60, and 100% relative humidity (RH). The stratified MEA Pt loading was reduced by 12% while maintaining commercial equivalent performance. The optimal two-layer design was achieved when the Pt loading ratio between the layers was 1:6 (inner:outer layer). This MEA showed the highest ECSA and performance at 0.65 V with reduced mass transport losses. The integrity of stratified MEAs with lower Pt loading was evaluated with potential cycling and proved more durable than the monolayer MEA equivalent. The higher ionomer loading adjacent to the membrane and the bi-layer interface of the stratified catalyst layer (CL) increased moisture in the cathode CL, decreasing the degradation rate. Using ionomer stratification to decrease the Pt loading in an MEA yielded a better performance compared to the monolayer MEA design. This study, therefore, contributes to the development of more durable, cost-effective MEAs for low-temperature proton exchange membrane fuel cells.

**Keywords:** proton exchange membrane fuel cell; cathode catalyst layers; ionomer loading; stratified cathode catalyst layers



**Citation:** Nondudule, Z.; Chamier, J.; Chowdhury, M. Effect of Stratification of Cathode Catalyst Layers on Durability of Proton Exchange Membrane Fuel Cells. *Energies* **2021**, *14*, 2975. <https://doi.org/10.3390/en14102975>

Academic Editor: Jin-Soo Park

Received: 5 February 2021

Accepted: 10 May 2021

Published: 20 May 2021

**Publisher's Note:** MDPI stays neutral with regard to jurisdictional claims in published maps and institutional affiliations.



**Copyright:** © 2021 by the authors. Licensee MDPI, Basel, Switzerland. This article is an open access article distributed under the terms and conditions of the Creative Commons Attribution (CC BY) license (<https://creativecommons.org/licenses/by/4.0/>).

## 1. Introduction

Proton exchange membrane fuel cells (PEMFCs) have attracted great attention in research and development due to their simplicity, low-temperature operation (50–100 °C), absence of pollutants, and higher power density (40–60%) compared to conventional internal combustion gasoline engines [1]. PEMFCs currently use platinum (Pt) (nanoparticles dispersed on carbon support) as a catalyst for the energy driving hydrogen oxidation reactions (HORs) and oxygen reduction reactions (ORRs), which significantly increases their manufacturing cost [2]. The ORR occurring at the cathode is about six orders of magnitude slower than the HOR requiring a higher Pt loading and is, therefore, the focal point for Pt reduction. Research and development activities are aimed at improving the catalyst activity and utilization in the cathode catalysts layer (CCL) without compromising durability and stability [3].

A promising MEA design includes the development of a graduated catalyst multilayer in the catalyst-coated membrane (CCM). A graduated CCL structure can increase the Pt catalyst use efficiency by increasing the available Pt surface area. Recent studies have shown that the O<sub>2</sub> mass transport resistance is inversely proportional to Pt loading and highly dependent on the available Pt surface area [4].

Many studies have focused on the CCL design to improve the MEA structure and materials' distribution in the CL [5–8]. They demonstrated that non-uniform CL structures can increase electrode performance compared to monolayer CLs, using the same catalyst and Pt loadings [9–13]. The non-uniform multilayer cathode proposed by Yoon et al. [5] improved the proton and electron conductivity and therefore the oxygen reduction in the CL, which increased the MEA performance. The double-layer design consisted of electrolyte-rich and -poor layers. The best of both was sought, in which the electrolyte-induced electron conduction resistance was minimized where the largest mass transport occurred, enabling increased access to catalyst sites. The ionomer level was increased closer to the membrane, where hydration and proton transfer were key to performance.

Using an ionomer gradient in the catalyst layer design increases the pore size distribution and improves water management in an MEA. Roshandel et al. [14] conducted a study on multilayer cathodes showing that the fuel cell performance is affected by the porosity in a gas diffusion electrode (GDE). Xie et al. [6] designed GDEs containing gradient Nafion (Aldrich) layers and found that cathode performance improved when the Nafion content was higher in the GDE towards the CL/membrane interface and lower towards the CL/gas diffusion layer (GDL) interface. The design maximized proton transport in the regions of greatest ion flux and porosity in the regions with increased gas transport. Kim et al. [15] designed anode and cathode CLs with gradient Nafion<sup>®</sup> content (EW1100, DuPont Inc., Wilmington, Delaware, USA) and varied Pt loading. The dual catalyst layer coated MEA showed better cell performance at the high current density region than the monolayer MEA did, illustrating the need for porosity or mass transport in the outer layer. Jung et al. [16] proposed an electrode composed of a highly phase-separated 1-methyl-2-pyrrolidinone (NMP)-based external layer and a lowly phase-separated glycerol-based inner layer. The proposed electrode resulted in increased cell performance in the high-current region. They later improved on their work [17], showing that controlled porosity and water movement can increase Pt use efficiency. The Pt loading in the inner and outer layers was reduced to 0.16 and 0.04 mg<sub>Pt</sub>/cm<sup>2</sup>, producing a current density at 0.6 V, four times larger than a monolayer equivalent MEA.

The ionomer (Nafion, Du Pont Inc., Wilmington, DE, USA)/catalyst (Pt/C) gradient design by Chen et al. [18] reported a 28.40 to 135.7% higher power density compared to the conventional single-layer CL MEA depending on the relative humidity. An increased power density was observed at lower relative humidity, illustrating the increased hydration offered by higher ionomer loadings closer to the membrane. Shahgaldi et al. [8] designed an ionomer gradient CCL that improved the Pt utilization by approximately 15% as well as reducing the mass and proton transport resistances compared to the monolayer CCL design.

It is evident that gradual stratification of the CCL increases MEA performance [6, 8, 11, 13, 15–18] by building the CL structure to consider mass movement, hydration, and access to active sites. This study investigates whether the durability of the MEA can be increased for the same considerations. Potential cycling of MEAs between 0 and 1.5 V (N<sub>2</sub>/H<sub>2</sub>) decreases the electrochemical surface area significantly due to both Pt dissolution and carbon corrosion [19]. Support corrosion in CCLs is one of the major contributors to the reduced stability and lifetime of PEMFCs [20]. The durability of the MEA decreases with decreasing CCL thickness and Pt loading [20], simply due to the lower availability of the support fuel (carbon) and the accelerated degradation of the catalyst layer's structural integrity. Stratification of the catalyst layer into electrolyte-rich and -poor cathode sublayers can increase its durability towards carbon corrosion. Superior water management closer to the membrane and reduced hydration in the outer layer closer to the gas diffusion layers will limit the movement of dissolved Pt into the membrane. The electrolyte-poor catalyst layer will likely be less prone to carbon corrosion due to the lower retained water content [19].

## 2. Materials and Methods

### 2.1. MEA Preparation

The catalyst ink was prepared by dispersing HySA-K40 (HyPlat<sup>®</sup>) Pt on carbon (Pt/C 40 wt. % Pt) in 99.9% isopropyl alcohol, deionized water, and Aquivion<sup>®</sup> ionomer (25.0 wt. % solids, D79-25BS Solvay, Princeton, NJ, USA). The catalyst slurry was coated onto a 50-cm<sup>2</sup> M820.15 gore membrane using the ultrasonic spray method. The ionomer content of the monolayer CCL design was 24 wt. %. For a stratified CCL design, two catalyst inks containing 24 and 28 wt. % ionomer contents were prepared. The first ink slurry, containing 28 wt. % ionomer, was sprayed onto the membrane to form the first layer until a targeted Pt loading was reached, as shown in Table 1. The second ink mixture, containing 24 wt. % ionomer, was deposited onto the first layer of catalyst to form the outer layer (Table 1). The cathode Pt loading was 0.4 mg<sub>Pt</sub>/cm<sup>2</sup> for the monolayer CCL and 0.35 mg<sub>Pt</sub>/cm<sup>2</sup> for the stratified CCL MEA design. The anode Pt loading was fixed at 0.1 mg<sub>Pt</sub>/cm<sup>2</sup> as a monolayer for both the monolayer and stratified CCL designs. After coating, the CCM was fitted with a gasket and hot pressed at 90 °C and 10,000 kPa for 1 min using a hot press to ensure complete sealing. The CCM fitted with a gasket was then sandwiched between two double-layer GDLs (Avcarb MB30) to form an MEA. The MEA thickness was then measured using a thickness gauge.

**Table 1.** Specifications of monolayer and stratified CCL designs.

	Cathode Pt Loading (mg <sub>Pt</sub> /cm <sup>2</sup> )		Total Cathode Pt Loading (mg <sub>Pt</sub> /cm <sup>2</sup> )	Ionomer Loading (wt. %)	
	Inner Layer	Outer Layer		Inner Layer	Outer Layer
MEA #1M	0.40	-	0.40	24	-
MEA #2M	0.35	-	0.35	24	-
MEA #3	0.050	0.30	0.35	28	24
MEA #4	0.10	0.25	0.35	28	24
MEA #5	0.15	0.20	0.35	28	24
MEA #6	0.20	0.15	0.35	28	24

### 2.2. Physical Characterization Techniques

The Brunauer–Emmett–Teller (BET) technique and a scanning electron microscopy (SEM) analysis were used to characterize the MEAs. The SEM images were taken with an FEI Nova NanoSEM 230 using a backscatter detector at 20.0 keV at 2000, 5000, and 10,000× magnification. The BET analysis was performed using a Micrometrics TriStar II 3020 to determine the surface area, pore size, and cumulative pore volume of the CLs.

### 2.3. Electrochemical Measurement

The MEA was placed into a 50-cm<sup>2</sup> single cell fuel cell hardware consisting of two graphite bipolar plates with parallel flow field channels, current collectors, and two end plates [21]. The assembly was compressed to a torque of 5 Nm.

All single cell tests were conducted with a fully automated FuelCon (C50-LT) fuel cell test station in the humidity range of 20–100% relative humidity (RH). The MEA was conditioned prior to polarization measurements: the cell was heated up to 80 °C at 100% RH, with hydrogen and airflow in the potential range between 0.3 and 1 V in potential steps of 0.05 V. Pure H<sub>2</sub> gas was supplied at 0.00111 Nm<sup>3</sup>/min to the anode and air at 0.00265 Nm<sup>3</sup>/min to the cathode compartment. The conditioning cycle was repeated 12 times for a 2-h period. The single cell was activated at 0.3 V using H<sub>2</sub> and air at 80% RH, a 74.6 °C operating temperature, and 2-bar back pressure for both the anode and cathode. Polarization (I–V) curves were measured at 80 °C while the cathode and anode were fed with air and pure H<sub>2</sub> with stoichiometries of 2.5 and 1.5, respectively. I–V curves were recorded at 20, 60, and 100% RH. Cyclic voltammograms (CVs) were collected under gas fluxes of 500 mL/min N<sub>2</sub> at the cathode and 300 mL/min H<sub>2</sub> at the anode at 80 °C from 20 to 100% RH. The potential scan range in the CV was 0.04–0.9 V, scanned at 50 mV/s. The hydrogen adsorption peak was then used to determine the electrochemical surface

area (ECSA). The EIS was measured in a frequency range from 20 kHz to 100 mHz with an amplitude of 5 mV while the cell was operated at 500 mA/cm<sup>2</sup> and 80 °C.

#### 2.4. Accelerated Stress Test

An accelerated stress test (AST) was used to study the durability of the support during potential cycling. The cell was conditioned at the conditions listed in Table 2.

**Table 2.** Fuel cell operating conditions for the carbon corrosion AST.

	Cell Temperature (°C)	Gas Flow Rates (Nl/min)	Feed Gas Temperature (°C)	Back Pressures (bar)	RH (%)
Standard operating conditions	80	1.11 H <sub>2</sub> (anode) 2.65 Air (cathode)	50 °C anode (H <sub>2</sub> ) 50 °C cathode (Air)	2	100 (anode) 80 (cathode)
Carbon corrosion test conditions	80	0.2 H <sub>2</sub> (anode) 30 N <sub>2</sub> (cathode)	83 °C anode (H <sub>2</sub> ) 83 °C cathode (N <sub>2</sub> )	1	100 (anode) 100 (cathode)

During the carbon corrosion test, carbon and water oxidation were incurred by cycling voltage across the MEA. The potential was cycled repeatedly between 0 and 1.2 V at 50 mv/s. The process was repeated for up to 6000 cycles. The experimental cycles were divided into the following segments: beginning of life (BoL), 20, 180, 200, 600, 1000, 2000, and 6000 cycles. Polarization curve, hydrogen crossover, and CV were measured after each segment.

### 3. Results and Discussion

#### 3.1. Reducing Pt Loadings in Stratified MEAs

The loading in the CCL was reduced to 0.35 mg<sub>Pt</sub>/cm<sup>2</sup> in a monolayer as well as stratified configurations. The thicknesses of the MEAs are presented in Table 3. The reduced Pt loading MEAs (MEA #2M- #6) were 16–40% thinner than the high Pt loading monolayer MEA #1M, mostly due to the decreased Pt loading. MEAs with a thicker 28 wt. % I loading layer (MEA #5 and #6) were thinner and relatively less porous than those with more 24 wt. % I (MEA #3 and #4). Increasing the ionomer loading in the CL impacted the agglomerate and aggregate size and distribution in the CL. Consequently, the stratified CCLs had dual Pt/C-ionomer layer structures due to their varying Pt/C to ionomer ratios as well as an interface boundary. Increasing the ionomer content increased the ionomer thin film around the agglomerate structures and decreased the pore volume between the agglomerate structures. The 28 wt. % I ionomer layer presented with overall denser catalyst layers.

**Table 3.** The thickness and pore characteristics of the monolayer and stratified CCL MEAs.

	MEA Thickness (mm)	Bulk Density (g/cm <sup>3</sup> )	Cumulative Pore Volume (cm <sup>3</sup> /g)	BET Surface Area (m <sup>2</sup> /g)	% Porosity
MEA #1M	0.05180	0.8157	0.1443	70.18	11.77
MEA #2M	0.03067	1.144	0.1040	70.43	11.85
MEA #3	0.04200	1.002	0.09620	67.27	9.640
MEA #4	0.04330	0.9566	0.1867	57.77	17.89
MEA #5	0.03700	1.141	0.04209	54.50	4.800
MEA #6	0.03800	1.111	0.09623	47.22	10.68

The BET surface areas of the monolayer MEAs were significantly higher compared to the stratified layers, which is primarily attributed to the nature of the deposition method. During monolayer coating, the layer is sprayed continuously in a single timeframe to achieve the desired thickness. While manufacturing stratified layers, a single ionomer ink is coated until the desired loading is reached. Thereafter, it rests until all the MEAs are completed. This provides a settling time for the first layer until a second layer, with a decreased ionomer content, can be deposited onto it. The second layers can therefore

penetrate the first to a larger extent, reducing the layer thickness and porosity as well as surface area.

The BET surface area of the stratified MEAs decreased with the increasing thickness of the first layer containing 28 wt. % ionomer. Thus, an increasing ionomer content increases the ionomer coverage in the CL and, therefore, the surface area.

### 3.1.1. Electrochemical Surface Area

Figure 1 presents the ECSAs of the stratified and non-stratified MEAs at full and 12% reduced Pt loading.

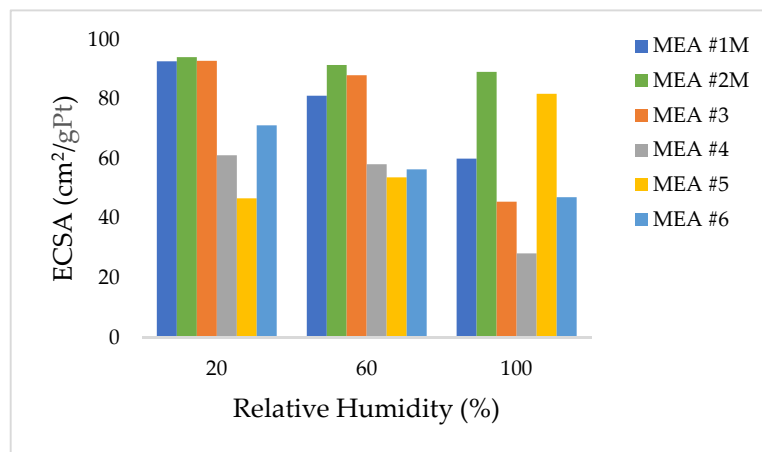


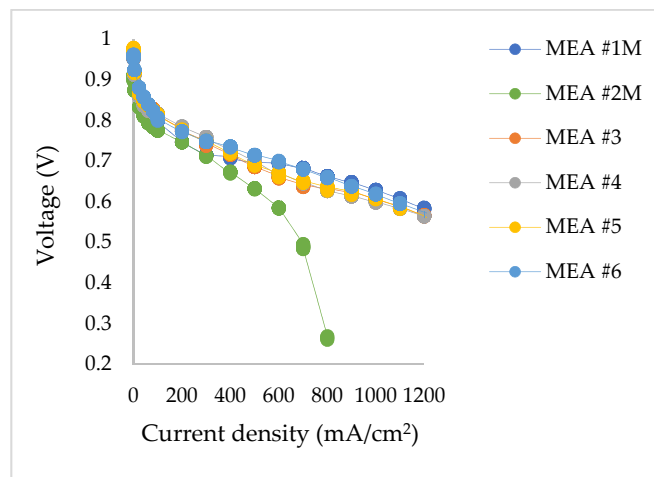
**Figure 1.** The ECSAs for the stratified and monolayer MEAs determined at 20–100% RH.

The monolayer MEA #2M, with reduced Pt loading, demonstrated the largest and most consistent ECSA under all RH conditions ( $94.11 \text{ m}^2/\text{g}_{\text{Pt}}$ ,  $91.52 \text{ m}^2/\text{g}_{\text{Pt}}$ , and  $89.19 \text{ m}^2/\text{g}_{\text{Pt}}$ ), owing to its highly porous agglomerate structure. No trend in ECSA was observed for the increase or decrease in ionomer-loaded layer thickness. The stratified CCL MEA with the largest BET surface area and more 24 wt. % I loading (MEA #3) demonstrated a larger ECSA from 20 to 60% RH conditions ( $92.92 \text{ m}^2/\text{g}_{\text{Pt}}$  and  $88.04 \text{ m}^2/\text{g}_{\text{Pt}}$ ) and low porosity and surface area. MEA #5 showed the highest ECSA ( $81.81 \text{ m}^2/\text{g}_{\text{Pt}}$ ) of the stratified MEAs at 100% RH. The increase in ECSA with RH was also reported by Fan et al. [22], who mainly attributed this trend to the improved contact area between Pt particles and water domains instead of the formation of new transport pathways. The low porosity and denser agglomerate structure of MEA #5 could have played a role in increasing the contact area between water domains and ionomer/catalyst aggregates.

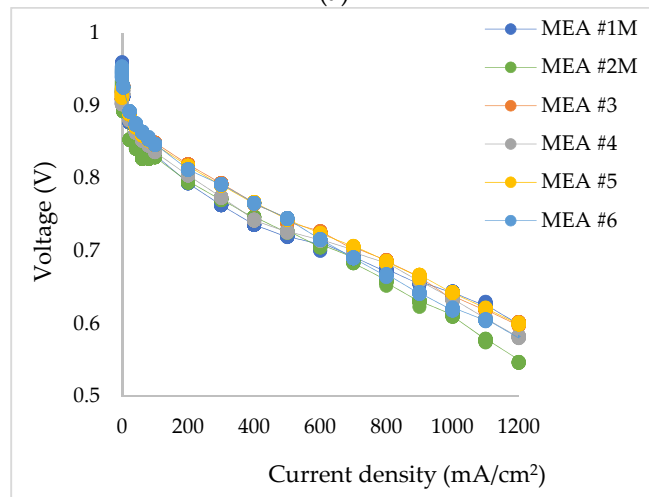
It is evident that the increased 28 wt. % I loading as well as the interface boundary of the dual catalyst layer structure impacted the ECSA. The higher ionomer content increased the surface coverage as well as water adsorption at higher relative humidity, which reduced access to Pt. The impact of the interface boundary layer, in which the second layer partially intrudes into the first, is also likely to have an impact on the overall access to catalyst active areas. This can be observed through the decreases in surface area and porosity of the stratified layers compared to the monolayer structures.

### 3.1.2. MEA Performance

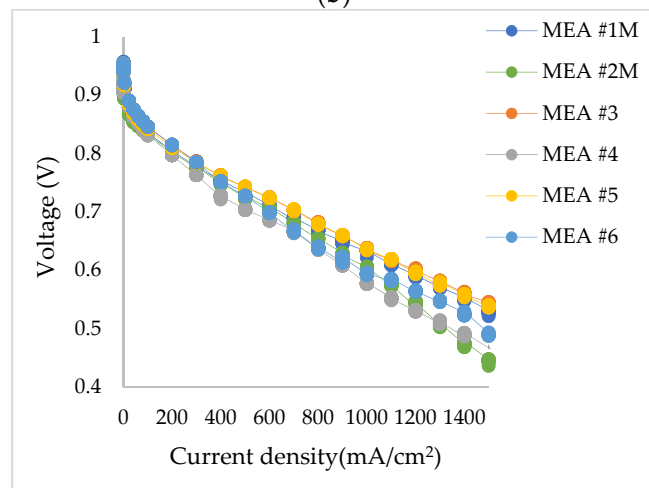
To determine the effect of ionomer stratified layers on the electrochemical performance of the resulting MEA, the polarization curves are compared in Figure 2.



(a)



(b)



(c)

**Figure 2.** Polarization curves for monolayer (MEA #1M and #2M) and stratified MEAs (MEA #3- #6) obtained for (a) 20% RH, (b) 60% RH, and (c) 100% RH.

The polarization curves in Figure 2 show that the output voltage performance decreased as the amount of current drawn from the single cell was increased. The output voltage was lowered by various resistances experienced through the MEA with increasing current density. At low current densities (<200 mA/cm<sup>2</sup>), a sharp decrease in output

voltage is observed due to activation losses. The intermediate region is the ohmic loss region ( $<600 \text{ mA/cm}^2$ ), and the high current density region ( $>1000 \text{ mA/cm}^2$ ) is the mass transport loss region. Ohmic losses represent a combination of ionic and electronic, membrane, and contact resistances. Mass transport losses in the high current density region are associated with gas diffusion limitations from the supply channels to the CL active sites where electrochemical reactions occur [23]. The stratified CCL MEAs performed better than the loading equivalent monolayer MEA #2M did in the high current density region. This performance improvement is attributed to the higher ionomer loading in the first layer, which increased proton conductivity, and a lower ionomer loading in the second layer, which reduced mass transport losses [8,11].

At low current densities ( $200 \text{ mA/cm}^2$  and lower), the activation losses of the monolayer MEA #2M were higher than those of the stratified MEAs, indicating limitations for charge transfer. Under dry conditions, the performance of the stratified MEAs improved with the increasing thickness of the 28 wt. % layer due to the increased ability to retain water. At low RH, MEA #6, which had the thickest 28 wt. % I layer, demonstrated superior performance owing to its higher proton conductivity. From medium to high current densities, the voltage drop was greater for MEA #2M under all RH conditions due to increased ionic transport resistances, which limited its performance. At high current densities, MEAs #4 and #6 experienced higher voltage losses, indicating mass transport-related losses. It is evident that the boundary interface between the catalyst layers did not have a uniform impact on the performance of the MEAs, save for improvement in the lower current density region. The lower losses indicate an increase in electronic connectivity, despite the overall decrease in ECSA for the stratified MEAs. Figure 3 compares the performances of the lower Pt loading MEAs (MEA #2M- #6) and the benchmark MEA #1M, with  $0.4 \text{ mg}_{\text{Pt}}/\text{cm}^2$  Pt loading. The performance was determined at  $0.65 \text{ V}$ —the voltage at which the benchmark performance for automotive design systems from ambient to saturated conditions (0–100% RH) is determined [24].

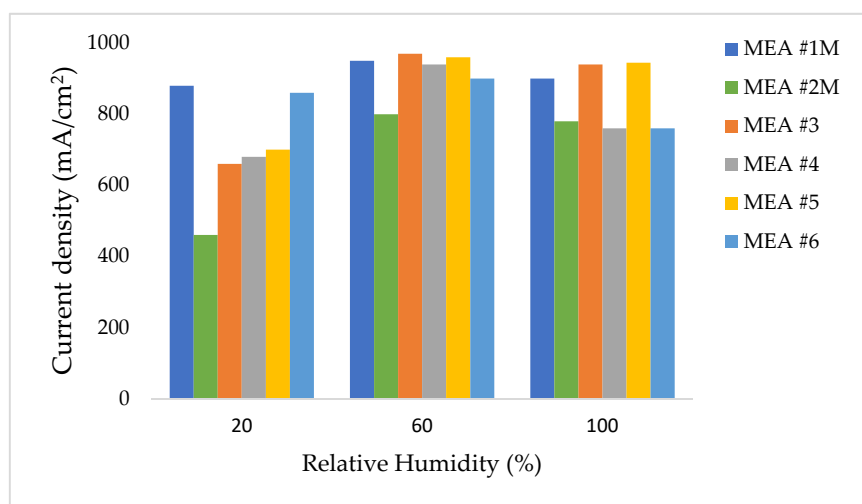


**Figure 3.** The current density ( $\text{mA/cm}^2$ ) for the stratified and non-stratified MEAs determined at 20–100% RH and  $0.65 \text{ V}$ .

Under dry conditions, MEA #2M demonstrated very poor performance ( $460 \text{ mA/cm}^2$ ), achieving 52.27% of MEA #1M's performance. The Pt utilization may have dropped significantly for the low Pt content 24 wt. % MEA due to the inefficient I/C ratio. As expected, the performance of the stratified MEAs decreased with a decrease in the first layer's thickness, as a higher ionomer loading decreases the ionic resistance under dry conditions. At higher RH, the ionomer absorbs moisture [25] and elongates ionic pathways. A higher ionomer loading means more hydrophilic zones and greater ionomer swelling, which increases charge transfer resistances at higher RH. As a result, when the RH increased, the perfor-

mance of MEAs with more 24 wt. % I loading increased (relative to higher 28 wt. % I). Lower ionomer loading on the secondary layer clearly contributed to improved mass transport, preventing water accumulation in the active area. Generally, the performance of the reduced Pt loading MEAs was comparable to the benchmark monolayer MEA #1M. It is, therefore, possible to reduce the Pt loading by 12% and still achieve a similar benchmark performance under various RH conditions in stratified catalyst layers. Sasikumar et al. [26] studied the dependence of ionomer content on Pt loading and found that the optimal ionomer content depends on the Pt loading. This study has confirmed that the performance in various RHs is strongly dependent on the I/C loading ratio. MEA #3 with a Pt ratio = 1:6 (0.05 1st layer and 0.3 2nd layer) gave the best performance at higher RH and MEA #5 with a 1:0.75 (0.15 1st layer and 0.2 2nd layer) ratio performed best under dry conditions.

### 3.1.3. EIS Analysis

To further understand the performance of the monolayer and stratified MEAs, EIS was used to determine the key resistances. The resulting Nyquist plots are presented in Figure 4, showing the imaginary impedance ( $Z''$ ) as a function of real impedance ( $Z'$ ). In the high-frequency range, ohmic resistances dominate, while the intermediate frequency region is dominated by kinetic and charge transfer resistances ( $R_{ct}$ ). Charge transfer resistances depend on interfacial reaction kinetics resulting from the three-phase boundary zone [27]. The magnitude of total ohmic resistance ( $R_{\Omega}$ ) of the cell is determined by the intercept of the high-frequency curve with the  $Z'$  real axis. The EIS spectrum generally shows two distinctive arcs representing the charge transfer resistance ( $R_{ct}$ ) and the mass transport resistance ( $R_{mt}$ ) [27]. Figure 4 shows the Nyquist plots obtained for the monolayer and stratified MEAs. The mass transfer resistance arc was reasonably small to insignificant in the Nyquist plots because the study was conducted at low current density ( $500 \text{ mA/cm}^2$ ), where charge transfer and ohmic resistances dominate. The resistance to charge transfer arc varies significantly at higher RH, suggesting that the higher humidity impacts the electron transfer, most likely by the formation of water barriers. At 100% RH, the smallest arcs were demonstrated by the monolayer MEAs, indicating that the boundary interface in the stratified layers has an impact on the charge transfer pathways. Meanwhile, ohmic resistance decreased with increasing RH for all MEAs. At low RH, the ohmic resistance varied significantly between MEAs, with the difference decreasing with increasing humidity. This is due to a reduction in ionic resistance through the membrane and the ionomer in the catalyst layer. At lower humidity, the contribution of the ionomer to hydration is more evident.

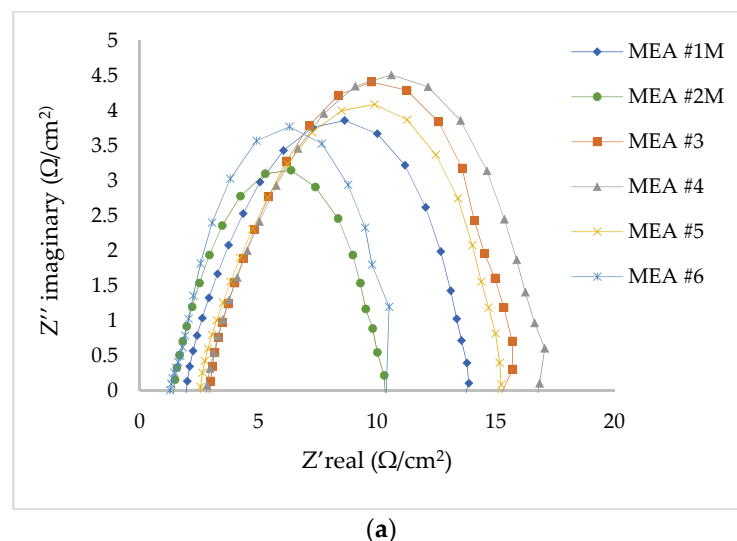
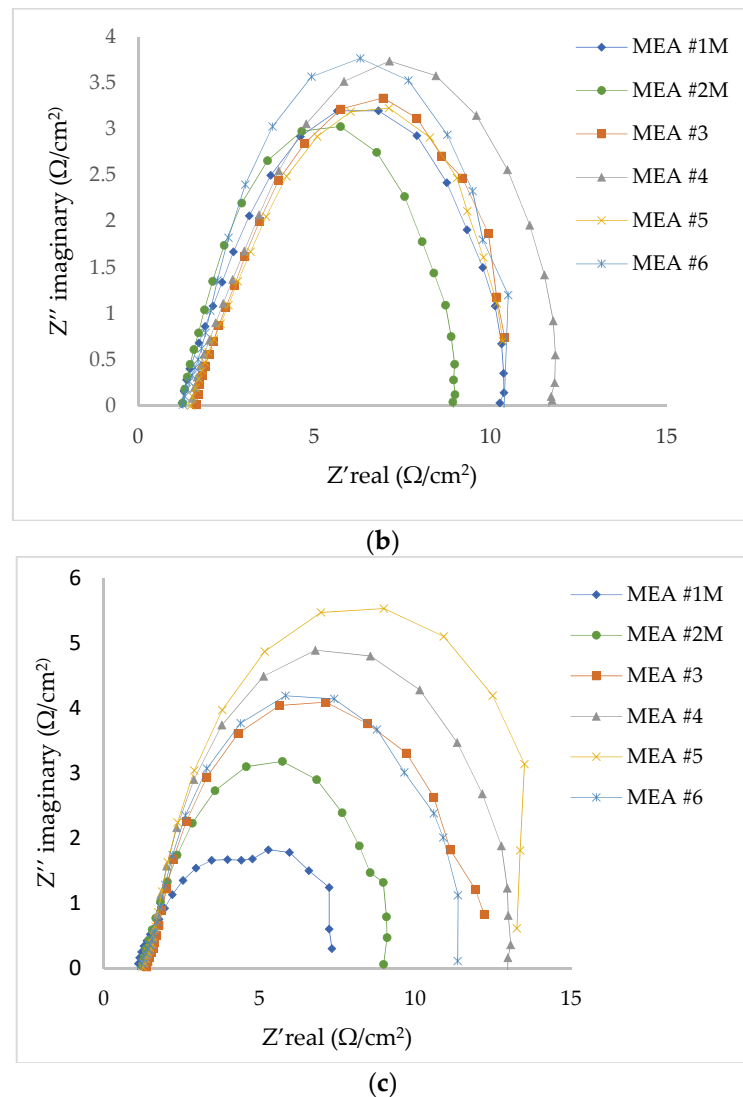


Figure 4. Cont.



**Figure 4.** Nyquist plots of benchmark monolayer MEA (MEA #1M) and reduced Pt loading MEAs (MEA #2M- #6), under (a) 20%, (b) 60%, and (c) 100% RH.

The Nyquist plots were fitted with a Randles equivalent circuit model [28] and the results are shown in Table 4. R1 represents the ohmic resistance and the charge transfer resistance is given by R2.

**Table 4.** The EIS fitting parameters obtained from the Randles equivalent circuit model.

		MEA #1M	MEA #2M	MEA #3	MEA #4	MEA #5	MEA #6
R1 ( $\Omega \text{ cm}^2$ )	20% RH	2.019	1.759	2.748	2.854	2.683	1.328
	60% RH	1.325	1.600	1.655	1.560	1.253	1.263
	100% RH	1.115	1.560	1.438	1.334	1.320	1.336
R2 ( $\Omega \text{ cm}^2$ )	20% RH	10.56	8.157	9.004	8.561	8.090	7.146
	60% RH	5.873	6.278	6.712	6.503	7.274	7.339
	100% RH	6.004	6.228	7.565	7.788	7.339	7.177

At 20% RH, the ohmic and charge transfer resistances were the highest for all MEAs due to the lower water content in the membrane. At lower humidity, the stratified MEAs demonstrated lower charge transfer resistances compared to the  $0.4 \text{ mg}_{\text{Pt}}/\text{cm}^2$  monolayer MEAs (MEA #1M) due to the increased ionomer loading in the first layer. In the stratified MEAs, charge transfer and ohmic resistances both decreased with the increasing ionomer

thickness of the first layer. Increasing the thickness of the first layer increased proton conductivity and thus reduced ohmic resistance. The lowest charge transfer and ohmic resistances of 7.146 and 1.328  $\Omega \text{ cm}^2$  were demonstrated by MEA #6, respectively, which confirmed the better performance of this MEA in dry conditions. A sublayer containing 28 wt. % I reduced the resistance experienced in dry conditions.

At 60% RH, charge transfer resistances decreased with the increasing 24 wt. % I layer thickness in stratified MEAs. This can be attributed to the reduced effect of ionomer swelling and covering of electrochemical conductive areas [29–31]. Monolayer MEAs had the smallest charge transfer resistances in fully humidified conditions. From 20 to 100% RH, charge transfer and ohmic resistances were significantly lower for the benchmark MEA #1M as it had a higher Pt loading, which increased ORR kinetics. MEA #2M exhibited larger ohmic resistance under all RH conditions, likely contributing to its poor performance. The results suggest that a monolayer with 24 wt. % I loading is not optimal for the 0.35  $\text{mg}_{\text{Pt}}/\text{cm}^2$  loaded MEAs; a higher ionomer loading may be required.

### 3.2. Durability Comparison of Stratified and Monolayer MEAs

While the stratified CCL MEAs performed better than the monolayer equivalent MEA #2M in certain conditions, the durability of stratified MEAs is yet to be established. An AST which incurs carbon degradation was performed to compare the durability of the stratified MEAs with monolayer MEA #1M and MEA #2M. MEA #6, which was more consistent in reaching performance targets under the studied RH conditions, was selected for comparison. Cyclic voltammetry, SEM, and polarization analyses were performed to determine the MEA durability during the AST, which caused carbon and water oxidation through potential cycling.

#### 3.2.1. Catalyst Layer Degradation

Cross-sectional images of the stratified and monolayer CCL MEAs before and after the 30-h AST are shown in the SEM images of Figure 5. The MEAs used for SEM imaging and those used in the AST differ due to the nature of the sample preparation. A 10% size variation is expected between MEAs of the same set due to the nature of the production process. The thicknesses are therefore qualitative values and only serve as an estimation of the catalyst layer integrity after the AST.

The CCL of the unused MEA #1M is thicker than those of MEA #2M and #6. The MEA #6 CCL was also 19.29% thicker than that of MEA #2M before the degradation test, owing to the high ratio of 28 wt. % ionomer layer on the inner layer of MEA #6. Figure 5b,d,f show the thinning of the CL structure of MEA #1M, #2, and #6 due to severe carbon degradation. The MEA thicknesses are summarized in Table 5.

After the carbon degradation test, thinning of both the anode and cathode CLs was observed for all MEAs. The anode CL thinned by 83.88% for the stratified MEA and 86.55% for the reduced Pt loading monolayer MEA #2M. There was no significant change in the anode thickness of MEA #1M (1.72%) over the degradation period. The CCL thickness of MEA #1M was reduced by 54.32%, that of MEA #2M was reduced by 79.69%, and the stratified CCL of MEA #6 by 59.16%. The Pt/C, ionomer, and membrane, together, comprise the mechanical strength of a CCM. Decreasing the amount of any of these materials decreases the mechanical strength of an MEA. The degradation of the CLs and membrane was greater for the reduced Pt loading MEAs compared to the higher Pt loading MEAs. MEA #2M and MEA #6 experienced membrane dehydration/thinning, while the higher Pt loading MEA #1M experienced membrane swelling. The PEM of MEA #1M expanded during the carbon corrosion test due to isotropic and anisotropic swelling [32]. The water content in the membrane imposed swelling and resulted in high mechanical stresses, which could have resulted in membrane failure and gas crossover [33–35]. The thinning of the PEM membrane observed for lower Pt loading MEAs resulted from thermal and chemical degradation of the membrane during the carbon degradation process. This degradation could result in both gas crossover and electrical shortening [36–38]. The PEM

thickness decreased by 49.61% for MEA #6 and 71.93% for MEA #2M. Sethruman et al. [37] showed that inadequate water content and high temperature accelerate membrane thinning. Therefore, the high ionomer loading adjacent to the membrane of the stratified MEA #6 played a role in reducing PEM degradation by retaining moisture closer to the PEM and improving heat dissipation.

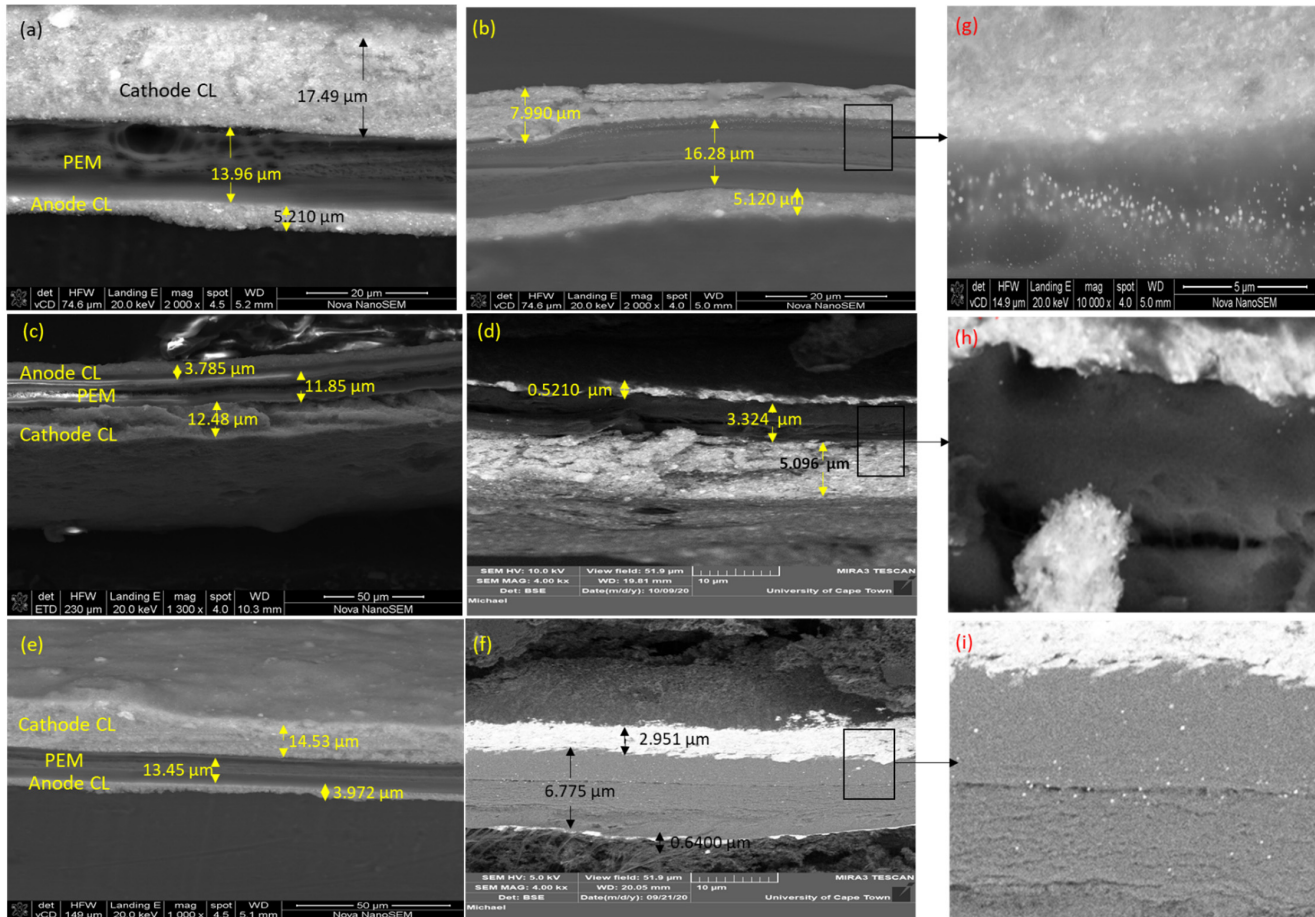


**Figure 5.** Cross-sectional images of an unused (a) CCL MEA #1M; (c) CCL MEA #2M; (e) CCL stratified MEA #6. After the carbon corrosion test, SEM images of the degraded (b) MEA #1M, (d) MEA #2M, and (f) MEA #6 were captured. Magnified images of the degraded (g) MEA #1M, (h) MEA #2M, and (i) MEA #6 show that Pt migrated from the CL into the PEM.

**Table 5.** The thicknesses of MEAs before and after the carbon degradation test.

	MEA Components	Thickness Before Degradation (μm)	Thickness After Degradation (μm)
MEA #1M	CCL	17.49	7.990
	PEM	13.96	16.28
	ACL	5.210	5.120
MEA #2M	CCL	12.48	5.029
	PEM	11.85	3.324
	ACL	3.785	0.5210
MEA #6	CCL	14.53	2.951
	PEM	13.47	6.785
	ACL	3.972	0.6400

Pt migration into the PEM was observed for all MEAs, but less for MEA #2M (Figure 5h) and MEA #6 (Figure 5i) compared to MEA #1M (Figure 5g). Pt aggregates

appear as white particles on the PEM shown in Figure 5g,i, which suggests that Pt migrated from the catalyst layer. As the carbon support degradation, Pt particles dissolve, migrate, and precipitate into the PEM, resulting in a loss of electrochemical activity in the CL. Pt in the membrane is electronically and ionically isolated and cannot be accessed by gas reactants, which leads to electrical performance degradation [20,38].

### 3.2.2. ECSA Loss

The loss of Pt was evaluated periodically during the AST to examine the effect of electrochemical carbon corrosion on the ECSA. The ECSA losses were normalized to its beginning-of-life (BoL) ECSA and the following equation was used:

$$\% \text{ ECSA loss} = \frac{ECSA_{BoL} - ECSA_{n\text{-th cycle}}}{ECSA_{BoL}} \times 100, \quad (1)$$

where  $ECSA_{BoL}$  is the ECSA at the beginning of life, and  $ECSA_{n\text{-th cycle}}$  is the measured ECSA after the  $n$ -th cycle. The comparison of ECSA in Figure 6 shows a decrease in ECSA for all MEAs with progressive cycling.

The ECSA decreased over the degradation period due to carbon support corrosion and Pt dissolution [39]. There was an accelerated decay in the ECSA for MEA #1M compared to MEAs #2M and #6, congruent with the results reported by Speder et al. [40]. This is likely due to the extensive loss of Pt resulting from extensive Pt dissolution, as observed in Figure 5g. MEA #1 reached a 100.0% ECSA loss after only 2000 cycles, while MEA #2M had a total loss of 80.10% after 6000 cycles and MEA #6 had only a 59.55% total ECSA loss. The ECSA of MEA #2M decreased significantly faster than that of MEA #6. The extensive loss of ECSA in MEA #2M resulted from a drastic PEM degradation, as observed in Figure 5d, which possibly increased hydrogen crossover [41].

### 3.2.3. Decrease in Electrochemical Performance

Polarization curves were drawn with 59% RH on both the anode and cathode, at periodic intervals during the degradation period. Figure 7 shows the performance curves of MEA #6 and the monolayer MEAs over the degradation period.

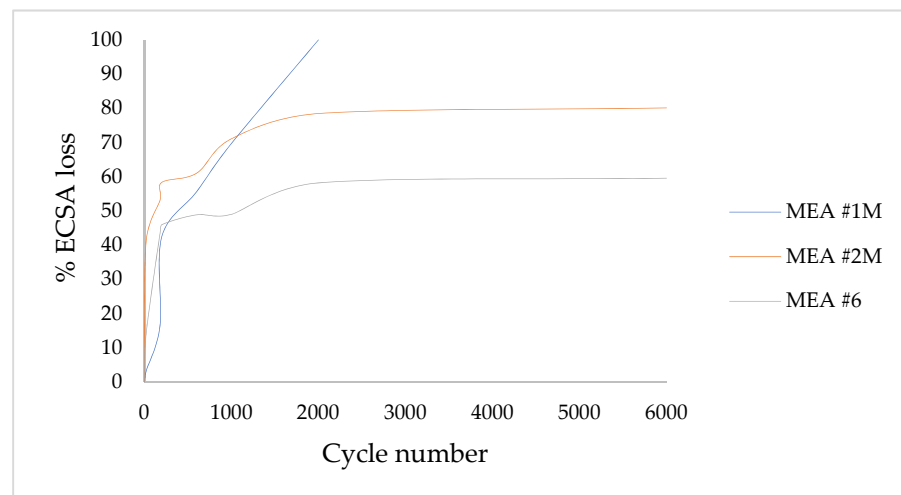
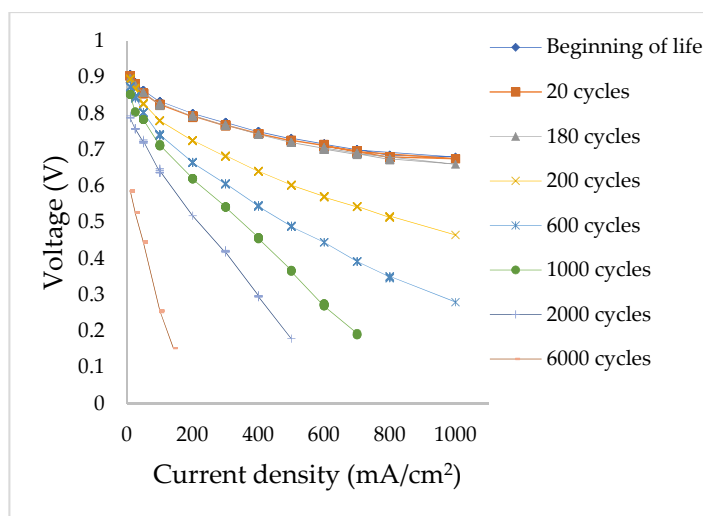
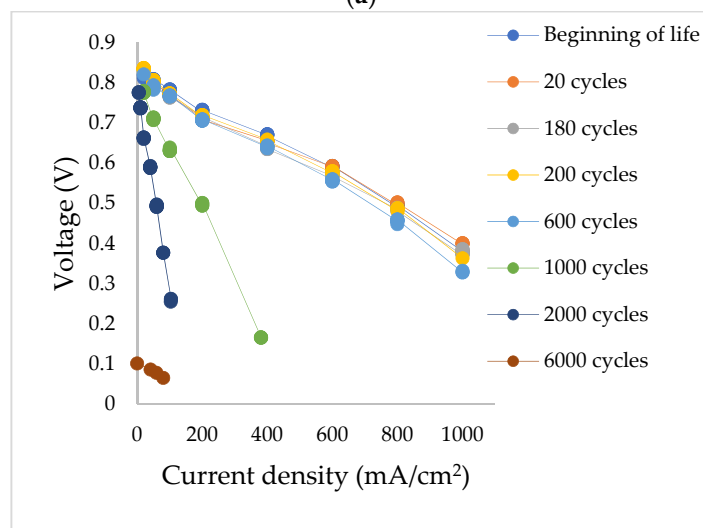


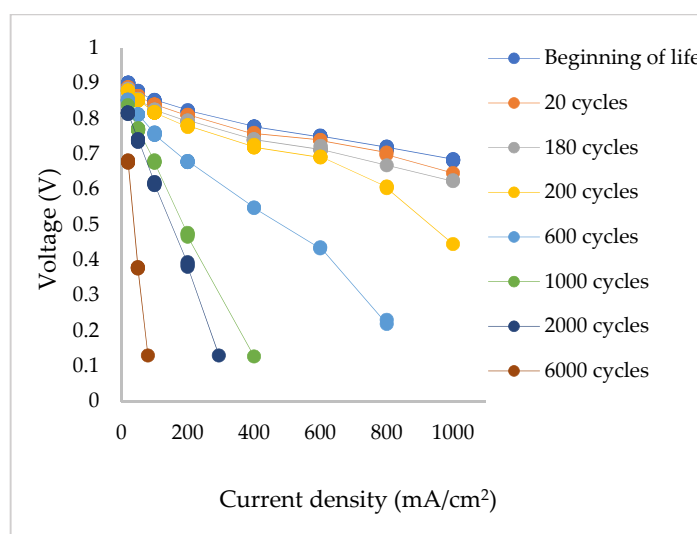
**Figure 6.** ECSA loss during cycling of the stratified MEA #6 and monolayer MEA #2M and MEA #1.



(a)



(b)



(c)

**Figure 7.** Performance curves taken during potential cycling for (a) MEA #1M, (b) MEA #2M, (c) and the stratified CCL MEA #6.

The performance curves show a decrease in cell potential after every following potential cycling period. The initial performance of the MEAs is comparable, but their performance degradation is distinctive. The output voltage decreased from the low to the high current density region with progressive cycling due to CL morphology changes caused by carbon degradation, mainly ECSA loss. Carbon degradation reduced the electron conduction, contributing to ohmic losses and charge transfer losses, while PEM degradation led to proton conductivity losses, all limiting performance. CL surface roughening due to carbon corrosion also contributes to the CL hydrophilicity and adds oxide groups resulting in oxygen diffusion and water management challenges, thus drastically reducing performance [42,43].

The OCV of MEA #2M drastically decreased after 6000 cycles from 0.8300 to 0.101 V, whereas that of MEA #6 OCV decreased from 0.9100 to 0.6800 V and that of MEA #1M from 0.8900 to 0.5850 V. These OCV losses can be correlated to increased hydrogen crossovers associated with membrane swelling/thinning [41,44] and Pt surface area losses during potential cycling.

To compare the performance losses obtained in each MEA, the voltage losses were normalized to the BoL cell voltage and the following equation was used [45]:

$$\% \text{ Performance loss} = \frac{V_{BoL} - V_{n-th \text{ cycle}}}{V_{BoL}} \times 100, \quad (2)$$

where  $V_{BoL}$  is the cell voltage at BoL, and  $V_{n-th \text{ cycle}}$  is the voltage after the  $n-th$  cycle. Figure 8 presents the percentage performance loss of each MEA versus the cycling period measured at 200 mA/cm<sup>2</sup>.

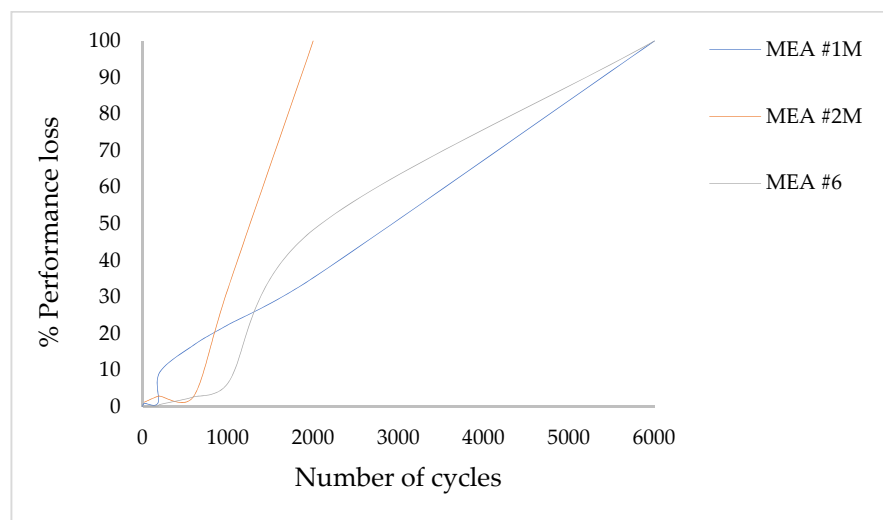


**Figure 8.** Percentage performance losses of the MEAs during potential cycling, measured at 200 mA/cm<sup>2</sup>.

Performance loss began to increase sharply after 1000 cycles for all MEAs. The higher Pt loading MEA #1M experienced lower performance losses at 200 mA/cm<sup>2</sup> compared to the reduced Pt loading MEAs. At 2000 cycles, MEA #2M reached 100.0% performance loss, while MEA #6 demonstrated 48.35% loss and MEA #1M, 35.25% loss.

Performance degradation was substantial for both the monolayer and stratified CCL MEAs, but the degradation of the CL after prolonged corrosion was slower in the MEAs with a stratified CCL with equivalent loading. This was corroborated by the higher ECSA, lower kinetic, and OCV losses after carbon degradation. The high ionomer coverage in the first layer of MEA #6 may have reduced carbon corrosion by retaining moisture closer to the membrane, preventing severe membrane dryness, which causes PEM degradation. The bilayer interface also played a role in enhancing the durability of the MEA by disrupting

the rate of mass transport during the carbon degradation test, thus reducing the carbon corrosion rate.

#### 4. Conclusions

Using an ionomer gradient approach, stratified CCL MEAs were designed for low-temperature PEMFCs. The goal of the project was to reduce Pt loading in the stratified layers without sacrificing performance and lifetime. This study has shown that using ionomer stratification to decrease the Pt loading in an MEA can yield better performance compared to the monolayer MEA equivalent, depending on the RH. Compared to the benchmark MEA at  $0.4 \text{ mg}_{\text{Pt}}/\text{cm}^2$ , the stratified MEA showed a  $\pm 2.00\%$  performance change from 20 to 60% RH and about a 13.00% performance increase in fully humidified conditions. This is in stark contrast to the 13.00 to 47.72% decrease in performance observed in the reduced Pt monolayer MEA compared to the commercial benchmark. Not only did the stratified MEA perform better than the monolayer equivalent MEA, but it also proved to be more durable.

The AST resulted in a decrease in the performance for each of the MEAs, which was correlated to a decrease in CCL thickness, membrane degradation, and ECSA loss. The stratified MEAs proved to be more durable than monolayer MEAs at equivalent Pt loadings. The high ionomer loading adjacent to the membrane of the stratified MEAs increases moisture in the CL, hydrating the PEM, and, therefore, slows the degradation process. Compared to the benchmark high Pt loading MEA, the stratified MEA showed increased durability by decreasing the ECSA loss by 41.83% and the OCV losses by 26.25%. However, a slight increase of 13.10% in kinetic losses was observed. The AST results showed that catalyst loading plays a major role in the durability of an MEA. Therefore, it is imperative to always consider the impact of reducing Pt loading on MEA durability. These findings are anticipated to contribute to the development of more durable MEAs for low-temperature PEMFCs. It is suggested that increasing the ionomer gap in stratified CCL MEAs and optimizing the ionomer content for low PGM MEAs could yield even better MEA performance and further increase MEA durability.

**Author Contributions:** Conceptualization, J.C. and Z.N.; methodology, Z.N. and J.C.; validation, Z.N. and J.C.; formal analysis, Z.N. and J.C.; investigation, Z.N. and J.C.; resources, J.C. and M.C.; data curation, Z.N. and J.C.; writing—original draft preparation, Z.N. and J.C.; writing—review and editing, Z.N., J.C. and M.C.; visualization, J.C. and Z.N.; supervision, J.C. and M.C.; project administration, J.C., Z.N. and M.C.; funding acquisition, J.C., Z.N. and M.C. All authors have read and agreed to the published version of the manuscript.

**Funding:** This research was funded by the National Research Foundation (NRF) Free Standing Innovation grant and HySA Catalysis funded by the South African Department of Science and Innovation.

**Data Availability Statement:** The data presented in this study are available on request from the corresponding author, J.C. upon request.

**Acknowledgments:** Special thanks to HyPlat (Pty) Ltd. for providing all materials used for the experiments in this study.

**Conflicts of Interest:** The funders had no role in the design of the study; in the collection, analyses, or interpretation of data; in the writing of the manuscript, or in the decision to publish the results.

#### References

1. Rajashekara, K.; Rathore, A.K. Power Conversion and Control for Fuel Cell Systems in Transportation and Stationary Power Generation. *Electr. Power Compon. Syst.* **2015**, *43*, 1376–1387. [[CrossRef](#)]
2. Zhang, J. (Ed.) *PEM Fuel Cell Electrocatalysts and Catalyst Layers*; Springer Science & Business Media: Vancouver, BC, Canada, 2008; pp. 88–89.
3. Ye, S.; Banham, D. Current Status and Future Development of Catalyst Materials and Catalyst Layers for Proton Exchange Membrane Fuel Cells: An Industrial Perspective. *ACS Energy Lett.* **2017**, *2*, 629–639.
4. Gasteiger, H.A.; Panels, J.E.; Yan, S.G. Dependence of PEM fuel cell performance on catalyst loading. *J. Power Sources* **2004**, *127*, 162–171. [[CrossRef](#)]

5. Yoon, Y.-G.; Yang, T.-H.; Park, G.-G.; Lee, W.-Y.; Kim, C.-S. A multi-layer structured cathode for the PEMFC. *J. Power Sources* **2003**, *118*, 189–192. [[CrossRef](#)]
6. Xie, Z.; Navessin, T.; Ken Shi, K.; Chow, R.; Wang, Q.; Song, D.; Andreausa, B.; Michael Eikerling, M.; Liua, Z.; Steven Holdcroft, S. Functionally Graded Cathode Catalyst Layers for Polymer Electrolyte Fuel Cells II. Experimental Study of the Effect of Nafion Distribution. *J. Electrochem. Soc.* **2005**, *152*, A1171–A1179. [[CrossRef](#)]
7. Su, H.-N.; Liao, S.-J.; Wu, Y.-N. Significant improvement in cathode performance for proton exchange membrane fuel cell by novel double catalyst layer design. *J. Power Sources* **2010**, *195*, 3477–3480. [[CrossRef](#)]
8. Shahgaldi, S.; Ozden, A.; Li, X.; Hamdullahpur, F. Cathode catalyst layer design with gradients of ionomer distribution for proton exchange membrane fuel cells. *Energy Convers Manag.* **2018**, *171*, 1476–1486. [[CrossRef](#)]
9. Wang, Q.; Eikerling, M.; Song, D.; Liu, Z. Structure and performance of different types of agglomerates in cathode catalyst layers of PEM fuel cells. *J. Electroanal. Chem.* **2004**, *573*, 61–69.
10. Sun, W.; Peppley, B.A.; Karan, K. An improved two-dimensional agglomerate cathode model to study the influence of catalyst layer structural parameters. *Electrochim. Acta* **2005**, *50*, 3359–3374. [[CrossRef](#)]
11. Srinivasarao, M.; Bhattacharyya, D.; Rengaswamy, R.; Narasimhan, S. Performance analysis of a PEM fuel cell cathode with multiple catalyst layers. *Int. J. Hydrog. Energy* **2010**, *35*, 6356–6365. [[CrossRef](#)]
12. Song, D.; Wang, Q.; Liu, Z.; Navessin, T.; Eikerling, M.; Holdcroft, S. Numerical optimization study of the catalyst layer of PEM fuel cell cathode. *J. Power Sources* **2004**, *126*, 104–111. [[CrossRef](#)]
13. Cetinbas, F.C.; Advani, S.G.; Prasad, A.K. Optimization of polymer electrolyte membrane fuel cell catalyst layer with bidirectionally-graded composition. *Electrochim Acta* **2015**, *174*, 787–798. [[CrossRef](#)]
14. Roshandel, R.; Farhanieha, B.; Saievar-Iranizad, E. The effects of porosity distribution variation on PEM fuel cell performance. *Renew. Energy* **2005**, *30*, 1557–1572. [[CrossRef](#)]
15. Kim, K.-H.; Kim, H.-J.; Lee, K.-Y.; Jang, J.H.; Lee, S.-Y.; Cho, E.; Oh, I.-H.; Lim, T.-H. Effect of Nafion gradient in dual catalyst layer on proton exchange membrane fuel cell performance. *Int. J. Hydrog. Energy* **2008**, *33*, 2783–2789. [[CrossRef](#)]
16. Jung, C.; Vahc, Z.Y.; Kim, T.; Yi, S. Investigation of the dual-layered electrode composed of catalyst layers with different phase separation levels for PEMFC. *Electrochim. Acta* **2014**, *196*, 495–502. [[CrossRef](#)]
17. Jung, C.Y.; Kim, S.K.; Lee, S.J.; Yi, S.C. Three-dimensional reconstruction of coarse dense catalyst layer for proton exchange membrane fuel cells. *Electrochim. Acta* **2016**, *211*, 142–147. [[CrossRef](#)]
18. Chen, G.; Wang, C.; Lei, Y.; Zhang, J.; Mao, Z.; Mao, Z.Q.; Guo, J.-W.; Li, J.; Ouyang, M. Gradient design of Pt/C ratio and Nafion content in cathode catalyst layer of PEMFCs. *Int. J. Hydrog. Energy* **2017**, *42*, 29960–29965. [[CrossRef](#)]
19. Dam, V.A.T.; De Bruijn, F.A. The stability of PEMFC electrodes: Platinum dissolution vs potential and temperature investigated by quartz crystal microbalance. *J. Electrochem Soc.* **2007**, *154*, B494. [[CrossRef](#)]
20. Yu, X.; Ye, S. Recent advance and durability advancement of Pt/C catalytic cathode in PEMFC Part II: Degradation mechanism and durability enhancement of carbon supported platinum catalyst. *J. Power Sources* **2007**, *172*, 145–154. [[CrossRef](#)]
21. Pollet, B.G.; Franco, A.A.; Liang, H.; Pasupathi, S. 1-Proton exchange membrane fuel cells. In *Compendium of Hydrogen Energy*; Woodhead Publishing Series in, Energy; Barbir, F., Basile, A., Veziroglu, T.N., Eds.; Woodhead Publishing: Oxford, UK, 2016; Volume 3, pp. 3–56.
22. Fan, L.; Wu, K.; Tongsh, C.; Zhu, M.; Xie, X.; Jiao, K. Mechanism of Water Content on the Electrochemical Surface Area of the Catalyst Layer in the Proton Exchange Membrane Fuel Cell. *J. Phys. Chem. Lett.* **2019**, *10*, 6409–6413. [[CrossRef](#)] [[PubMed](#)]
23. Yousfi-Steiner, N.; Moçotéguy, P.H.; Candusso, D.; Hissel, D.; Hernandez, A.; Aslanides, A. A review on PEM voltage degradation associated with water management: Impacts, influent factors and characterization. *J. Power Sources* **2008**, *183*, 260–274. [[CrossRef](#)]
24. Debe, M. Electrocatalyst approaches and challenges for automotive fuel cells. *Nature* **2012**, *486*, 43–51. [[CrossRef](#)] [[PubMed](#)]
25. Xu, H.; Song, Y.; Kunz, H.; Fenton, J. Effect of Elevated Temperature and Reduced Relative Humidity on ORR Kinetics for PEM Fuel Cells. *J. Electrochem. Soc.* **2005**, *152*, A1828–A1836. [[CrossRef](#)]
26. Sasikumar, G.; Ihm, J.W.; Ryu, H. Optimum Nafion content in PEM fuel cell electrodes. *Electrochim. Acta* **2004**, *50*, 601–605. [[CrossRef](#)]
27. Taillades, G.; Taillades-Jacquín, M.; Mauvy, F.; Essouhmi, A.; Marrony, M.; Lalane, C.; Fourcade, S.; Jones, D.J.; Greiner, J.-C.; Rozière, J. Intermediate Temperature Anode-Supported Fuel Cell Based on BaCe<sub>0.9</sub>Y<sub>0.1</sub>O<sub>3</sub> Electrolyte with Novel Pr<sub>2</sub>NiO<sub>4</sub> Cathode. *Fuel Cells* **2010**, *10*, 166–173.
28. Uygun, Z.O.; Uygun, H.D.E. A short footnote: Circuit design for faradaic impedimetric sensors and biosensors. *Sens. Actuators B Chem.* **2014**, *202*, 448–453. [[CrossRef](#)]
29. Lee, S.J.; Mukerjee, S.; McBreen, J.; Rhob, Y.W.; Khob, Y.T.; Lee, T.H. Effects of Nafion impregnation on performances of PEMFC electrodes. *Electrochim. Acta* **1998**, *43*, 693–701. [[CrossRef](#)]
30. Scibioh, M.A.; Oh, I.; Lim, T.; Hong, S.; Ha, H.Y. Investigation of various ionomer-coated carbon supports for direct methanol fuel cell applications. *Appl. Catal. B Environ.* **2008**, *77*, 373–385. [[CrossRef](#)]
31. Ma, S.; Solterbeck, C.; Odgaard, M.; Skou, E. Microscopy studies on proton exchange membrane fuel cell. *Appl. Phys. A* **2009**, *96*, 581–589. [[CrossRef](#)]
32. Kusoglu, A.; Karlsson, A.; Santare, M.; Cleghorn, S.; Johnson, W. Mechanical response of fuel cell membranes subjected to a hydro-thermal cycle. *J. Power Sources* **2007**, *161*, 987–996. [[CrossRef](#)]

33. Norin, L.; Kostecki, R.; McLarnon, F. Study of Membrane Degradation in High Power-Lithium Ion Cells. *Electrochem. Solid-State Lett.* **2002**, *5*, A67–A69. [[CrossRef](#)]
34. Solasi, R.; Zou, Y.; Huang, X.; Reifsnider, K.; Condit, D. On mechanical behavior and in-plane modeling of constrained PEM fuel cell membranes subjected to hydration and temperature cycles. *J. Power Sources* **2007**, *167*, 366–377. [[CrossRef](#)]
35. Yuan, X.; Liu, H.; Zhang, S.; Martin, J.; Wang, H. A review of polymer electrolyte membrane fuel cell durability test protocols. *J. Power Sources* **2011**, *196*, 9107–9116. [[CrossRef](#)]
36. Jourdan, M.; Mounir, H.; Marjani, R.E. Compilation of Factors Affecting Durability of Proton Exchange Membrane Fuel Cell (PEMFC). In Proceedings of the 2014 International Renewable and Sustainable Energy Conference (IRSEC), Ouarzazate, Morocco, 17–19 October 2014; pp. 542–547.
37. Sethuraman, V.A.; Weidner, J.W.; Haug, A.T.; Protsailo, L.V. Durability of Perfluorosulfonic Acid and Hydrocarbon Membranes: Effect of Humidity and Temperature. *J. Electrochem. Soc.* **2008**, *155*, B119. [[CrossRef](#)]
38. Dubau, L.; Castanheira, L.; Chatenet, M.; Maillard, F.; Dillet, J.; Maranzana, G.; Abbou, S.; Lottin, O.; De Moor, G.; El Kaddouri, A.; et al. Carbon corrosion induced by membrane failure: The weak link of PEMFC long-term performance. *Int. J. Hydrog. Energy* **2014**, *39*, 21902–21914. [[CrossRef](#)]
39. Oh, H.; Lee, J.; Kim, H. Electrochemical carbon corrosion in high temperature proton exchange membrane fuel cells. *Int. J. Hydrog. Energy* **2012**, *37*, 10844–10849. [[CrossRef](#)]
40. Speder, J.; Zana, A.; Spanos, I.; Kirkensgaard, J.J.K.; Mortensen, K.; Hanzlik, M.; Arenz, M. Comparative degradation study of carbon supported proton exchange membrane fuel cell electrocatalysts—The influence of the platinum to carbon ratio on the degradation rate. *J. Power Sources* **2014**, *261*, 14–22. [[CrossRef](#)]
41. Zhang, H.; Li, J.; Tang, H.; Lin, Y.; Pan, M. Hydrogen crossover through perfluorosulfonic acid membranes with variable side chains and its influence in fuel cell lifetime. *Int. J. Hydrog. Energy* **2014**, *39*, 15989–15995. [[CrossRef](#)]
42. Spornjak, D.; Fairweather, J.; Mukundan, R.; Rockward, T.; Borup, R.L. Influence of the microporous layer on carbon corrosion in the catalyst layer. *J. Power Sources* **2012**, *214*, 386–398. [[CrossRef](#)]
43. Park, J.-H.; Yim, S.-D.; Kim, T.; Park, S.-H.; Yoon, Y.-G.; Park, G.-G.; Yang, T.-H.; Park, E.-D. Understanding the mechanism of membrane electrode assembly degradation by carbon corrosion by analyzing the microstructural changes in the cathode catalyst layers and polarization losses in proton exchange membrane fuel cell. *Electrochim. Acta* **2012**, *83*, 294–304. [[CrossRef](#)]
44. Vielstich, W.; Lamm, A.; Gasteiger, H. Fundamentals, technology, applications. In *Handbook of Fuel Cells*; Wiley: Chichester, UK, 2003; Volume 3, p. 538.
45. Dhanushkodi, S.R.; Tamb, M.; Kundu, S.; Fowler, M.W.; Pritzker, M.D. Carbon corrosion fingerprint development and deconvolution of performance loss according to degradation mechanism in PEM. *J. Power Sources* **2013**, *240*, 114–121. [[CrossRef](#)]